Verification of solid hydrometeor properties simulated by a cloud resolving model using passive microwave radiometer and radar observations

Hisaki Eito and Kazumasa Aonashi

Meteorological Research Institute, Japan Meteorological Agency, Tsukuba, Japan

1. Introduction

Cloud resolving models (CRMs) with complicated cloud microphysical parameterizations explicitly predict various hydrometeors at high time and space resolution; therefore, CRMs serve as valuable tools for satellite remote sensing of precipitation for inferring information about precipitating clouds that cannot be directly observed. However, cloud microphysical validation of CRMs has not sufficiently been carried out. In this study, a CRM, the Japan Meteorological Agency (JMA) nonhydrostatic mesoscale model (JMA-NHM, Saito et al. 2006) is used to simulate typical moderate rainbands associated with the Baiu front observed around the Okinawa Islands, Japan on 8 June 2004. Microwave brightness temperatures (TBs) and equivalent radar reflectivities are derived from the model output, and are then compared to concurrent corresponding satellite radiometer (AMSR-E, Kawanishi et al. 2003) and ground-based radar (COBRA, Nakagawa et al. 2003) observations. The objectives of this study are to verify the two-moment bulk microphysics of the JMA-NHM and to examine some of the microphysical sensitivities. Special attention is given to the characteristics and sensitivities of frozen hydrometeor properties simulated by the JMA-NHM.

2. Models

The JMA-NHM is an operational nonhydrostatic mesoscale model developed by the JMA. Observed rainbands are simulated with one-way double-nested domains having horizontal grid sizes of 5 and 2 km. The same physical parameterization is used for the double-nested domains, except that the Kain-Fritcsh convective parameterization scheme is not used in the inner domain. An explicit three-ice bulk microphysics scheme (Ikawa and Saito 1991) is incorporated. This scheme predicts the mixing ratios of six water species (water vapor, cloud water, rain, cloud ice, snow and graupel) and number concentrations of ice particles. The size distributions for each precipitation particles are represented by exponential functions.

The radiative transfer model (RTM) developed by Liu (1998), which uses plane-parallel and spherical particle approximations, is used to simulate TBs in this study. TBs are obtained for each grid using the RTM interfaced with the JMA-NHM simulations. The simulated TBs are convolved with a Gaussian function that is close to the actual AMSR-E antenna patterns for each frequency, and then compared to concurrent corresponding AMSR-E observations.

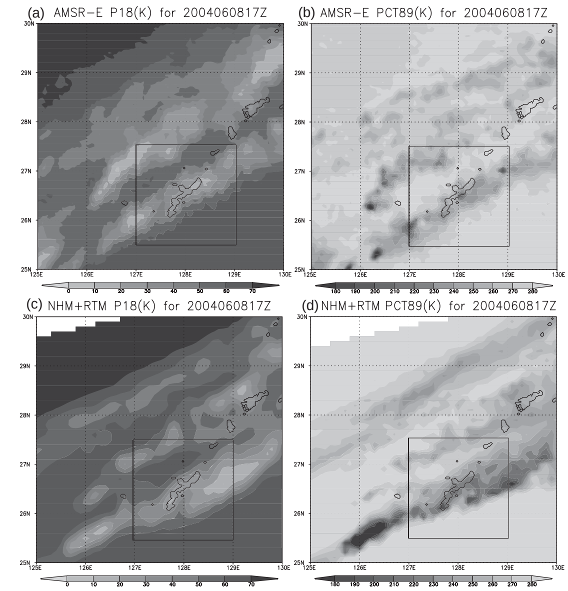

Fig. 1. (a) P18 and (b) PCT89 retrieved from TBs observed by AMSR-E at 17 UTC on 8 June 2004. (c) P18 and (d) PCT89 retrieved from TBs simulated by the JMA-NHM at 17 UTC on 8 June 2004. The rectangles represent the location of the area analyzed in Fig. 4.

3. Comparisons of simulations with observations

Figure 1a shows the polarization difference (vertically polarized TB minus horizontally polarized TB) at 18.7 GHz (P18) observed by AMSR-E at 1700 UTC on 8 June 2004. A P18 approaching zero corresponds to increasing absorption by rain and cloud water particles. Areas with low values of P18 are found in the rainbands, indicating the presence of large amounts of liquid water. The polarization-corrected temperatures (PCTs, Spencer et al. 1989) retrieved from the 89.0 GHz TB (PCT89) are presented in Fig. 1b. The depression of PCT89 is caused by scattering by frozen hydrometeors. Areas with depressions in PCT89 are also found in the rainbands, denoting that frozen hydrometeors also exist in those bands. Figures 1c and 1d depict P18 and PCT89 simulated by the JMA-NHM and RTM at 1700 UTC on 8 June 2004. The values of simulated P18 are almost in agreement with those of the AMSR-E observations. However, the simulated PCT89 depression is larger than the observed one. This result suggests that the JMA-NHM adequately simulates the amount of liquid hydrometeors; however, it overestimates the amount of frozen hydrometeors.

The JMA-NHM and COBRA data are compared using a statistical technique, contoured frequency with altitude diagrams (CFADs, Yuter and Houze 1995). Figure 2a depicts the reflectivity CFAD obtained from the COBRA observations. The highest probabilities follow a coherent pattern with the peak density gradually decreasing with height from between 25 and 35 dBZ near the melting level (about 4.5 km in height) to between 10 and 20 dBZ near the storm top at 13 km. Below the melting level, peak probabilities are almost constant to the surface. Figure 2b depicts the reflectivity CFAD obtained by the JMA-NHM simulation. Overall, good agreement is observed between the observations and the simulation. The highest probabilities also demonstrate a coherent pattern with peak densities similar to those of the observations. Below the melting level, peak probabilities for the simulated reflectivities agree with those from the observation. However, peak probabilities from the simulation appear to shift slightly higher above the melting level. This result suggests that model captures the observed reflectivities in the liquid phase fairly well; however, it slightly overestimates the size of hydrometeors in the ice phase.

The dominant form of ice in the simulation was snow with much smaller amounts of graupel and cloud ice (not shown). It seems reasonable that the dominant form of frozen hydrometeors is snow in this case; however, comparison with radar and radiometer data indicates that the amount of model-simulated snow is probably too large. This was caused by the JMA-NHM overestimation of the amount of snow through depositional growth (not shown).

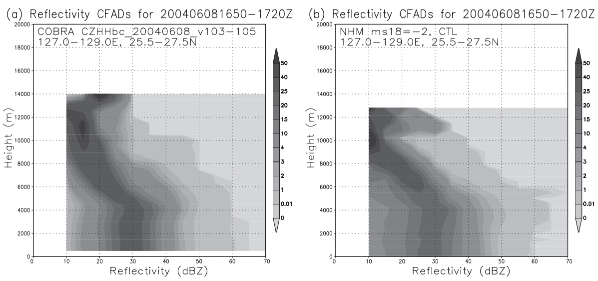

Fig. 2. Reflectivity CFADs for the region of 127–129°E, 25.5–27.5°N and the period from 1650 to 1720 UTC on 8 June 2004 derived from (a) the observed CORBA radar reflectivity data and (b) the JMA-NHM simulation.

4. Sensitivity experiments

As discussed in the previous section, comparisons with radar and radiometer observations suggest that the model overestimates the size and amount of snow. Based on those results, we conduct three sensitivity experiments (experiment IN, experiment PSACW, and experiment FVS) that involve adjustments to the snow microphysical parameters to quantify the process sensitivities in order to reduce excessive snow in the control experiment. In experiment IN, the ice nucleation process is changed to reduce the ice nucleation rate. This change reduces the depositional growth of snow due to a reduction in the number concentration of snow generated by the conversion of cloud ice. In experiment PSACW, the riming threshold for snow to graupel conversion is changed so that almost all of the accreted cloud water is converted into graupel. In experiment FVS, a higher snow fall speed is used so that snow particles quickly sediment out.

The mixing ratios of snow in all the sensitivity experiments are reduced from the control experiment (not shown), indicating that each adjustment has a positive impact in reducing the excessive snow. In experiments PSACW and FVS, the mean diameter is also reduced from the control experiment (not shown), due to the reduction in snow mixing ratios. In contrast, the mean diameter in experiment IN becomes larger than that of the control experiment (not shown), due to the large reduction in snow number concentration.

Profiles of probability density of the observed and simulated radar reflectivities for two levels at heights of 2.0 and 7.0 km are presented in Fig. 3. At a height of 2.0 km (Fig. 3a), under the melting level, the profiles for the sensitivity experiments are similar to those of the control experiment and the radar observations. At a height of 7.0 km (Fig. 3b), above the melting level, the peak probabilities at 20 dBZ in experiments PSACW and FVS shift closer to the observed value. In contrast, the peak probability at 25 dBZ in experiment IN remains similar to that of the control experiment and still shifts higher than the radar value.

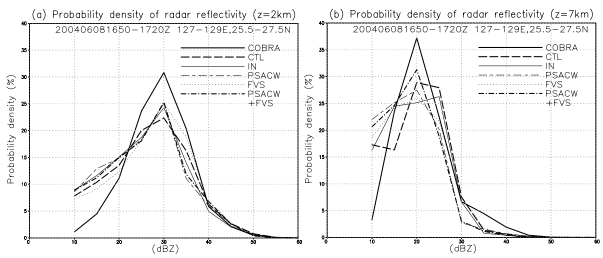

Fig. 3. Probability densities of reflectivity for the region of 127–129°E, 25.5–27.5°N at 1700 UTC on 8 June 2004 at a height of (a) 2 km and (b) 7 km. The probability density derived from the observed CORBA radar reflectivity data is denoted by the solid line, and the JMA-NHM simulations are denoted by the dashed line (the control experiment), thin solid line (experiment IN), short-long dashed line (experiment PSACW), dotted line (experiment FVS), and dot-dashed line (experiment PSACW+FVS).

Profiles of probability densities for P18 and PCT89 are presented in Fig. 4. The profiles of P18 in the sensitivity experiments shift closer to those in the observations (Fig. 4a). As indicated in Fig. 4b, probabilities of PCT89 less than 210 K in experiment

PSACW are slightly smaller than those for the control experiment, indicating that experiment PSACW performs better for reducing the overdepression of PCT89. In experiment FVS, fewer PCT89 values less than 230 K occur than in the control experiment, in better agreement with the observation.

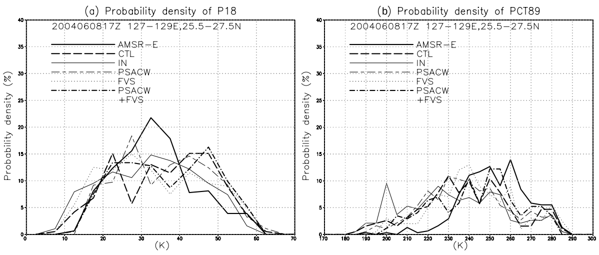

Fig. 4. Probability densities of (a) P18 and (b) PCT89 for the region of 127–129°E, 25.5–27.5°N at 17 UTC on 8 June 2004. Probability densities derived from the observed AMSR-E data are indicated by the solid lines, and the JMA-NHM simulations are denoted by the dashed line (the control experiment), thin solid line (experiment IN), short-long dashed line (experiment PSACW), dotted line (experiment FVS), and dot-dashed line (experiment PSACW+FVS).

Based on these results, an additional experiment is conducted using both adjustments to the microphysical parameters from experiments PSACW and FVS (experiment PSACW+FVS). Experiment PSACW+ FVS performs better for reducing the excessive amount and size of snow (not shown). As a result, experiment PSACW+FVS also performs better for reducing overdepression of PCT89 (Fig. 4b). Moreover, above the melting level, reflectivities of 20 dBZ occur more frequently in experiment PSACW+FVS than in the other experiments, in better agreement with the radar observations (Fig. 3b). However, the probabilities of PCT89 less than 230 K even in experiment PSACW+ FVS remain greater than were observed. These results suggest that the amount of snow is still excessive and that further adjustment to and improvement of the snow microphysical processes are necessary.

5. Summary

TBs and reflectivities simulations were conducted for rainbands around Okinawa Islands, Japan, which were compared to the timely corresponding AMSR-E and COBRA observations. Fairly good agreement was obtained between the simulation and observations in liquid phase, indicating that the JMA-NHM adequately simulated the amount of liquid hydrometeors. The intensity of scattering in the simulations was stronger than that in the observations above the melting layer, due to the fact that the JMA-NHM overestimated the amount and size of snow particles as a result of large depositional growth. The excessive snow contents were reduced by adjusting some of the microphysical processes in the JMA-NHM: the snowfall speeds were increased and a riming threshold for snow to graupel conversion was changed.

More analyses of many more situations and events are needed to estimate the generality of the model verification and microphysical sensitivities of the JMA-NHM presented in this study.

Acknowledgements

The authors express their thanks to Koyuru Iwanami of the National Research Institute for Earth Science and Disaster Prevention and Katsuhiro Nakagawa, Hiroshi Hanado, Yasushi Kitamura and Yukari Shusse of the National Institute of Information and Communications Technology for supplying the COBRA data. This study was partially supported by the Japan Aerospace Exploration Agency. The numerical experiments were performed using the SX-6 computer at the Meteorological Research Institute.

References

Ikawa, M. and K. Saito, 1991: Description of a nonhydrostatic model developed at the Forecast Research Department of the MRI. *Tech. Rep. MRI*, **28**, 238 pp.

Kawanishi, T., and Coauthors, 2003: The Advanced Microwave Scanning Radiometer for the Earth Observing System (AMSR-E), NASDA's contribution to the EOS for global energy and water cycle studies. *IEEE Trans. Geosci. Remote Sens.*, **41**, 184–194.

Liu G. 1998: A fast and accurate model for microwave radiance calculations. *J. Meteor. Soc. Japan*, **76**, 335–343.

Nakagawa, K., and Coauthors, 2003: Development of a new C-band polarimetric Doppler weather radar in Japan. *Proc. 23rd IGARSS*, 4462–4464.

Saito, K., and Coauthors, 2006 : The operational JMA nonhydrostatic model. *Mon. Wea. Rev.*, **134**, 1266–1298.

Spencer, R. W., H. M. Goodman, and R. E. Hood, 1989: Precipitation retrieval over land and ocean with the SSM/I: Identification and characteristics of the scattering signal. *J. Atmos. Ocean. Tech.*, **6**, 254–273.

Yuter, S. E. and R. A. Houze Jr., 1995: Three-dimensional kinematic and microphysical evolution of Florida cumulonimbus. Part II: Frequency distributions of vertical velocity, reflectivity, and differential reflectivity. *Mon. Wea. Rev.*, **123**, 1941–1963.